Supporting Information

Deep Dehalogenation of Florfenicol Using Crystalline CoP Nanosheet Arrays on a Ti Plate via Direct Cathodic Reduction and Atomic H

Huiling Liu,[†] Jinglong Han,[‡] Jili Yuan,[†] Chengbin Liu,[†,*] Dong Wang,[#] Tian Liu,[†] Meijun Liu,[†] Jinming Luo,[#,*] Aijie Wang,[‡] and John C. Crittenden[#]

[†] State Key Laboratory of Chemo/Biosensing and Chemometrics, Hunan University, Changsha 410082, P. R. China

[‡] Research Center for Eco-Environmental Sciences, Chinese Academy of Sciences, Beijing 100085, P.R. China

[#] Brook Byers Institute for Sustainable Systems and School of Civil and Environmental Engineering, Georgia Institute of Technology, 828 West Peachtree Street, Atlanta, Georgia 30332, United States

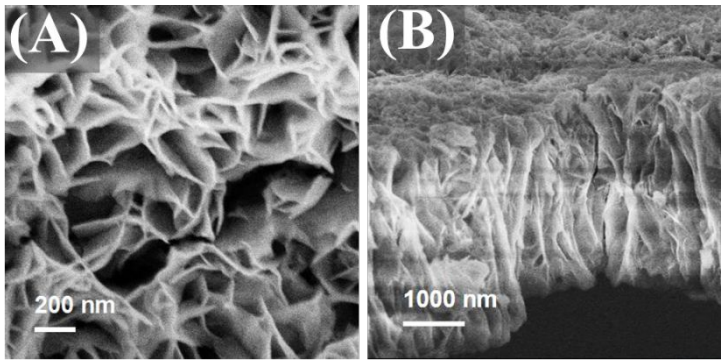

Figure S1. SEM images of the $Co(OH)_2$ nanosheet arrays

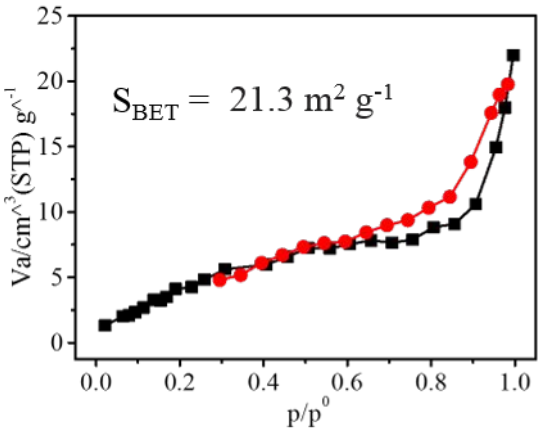

Figure S2. Nitrogen adsorption/desorption isotherm plot of C-CoP/Ti.

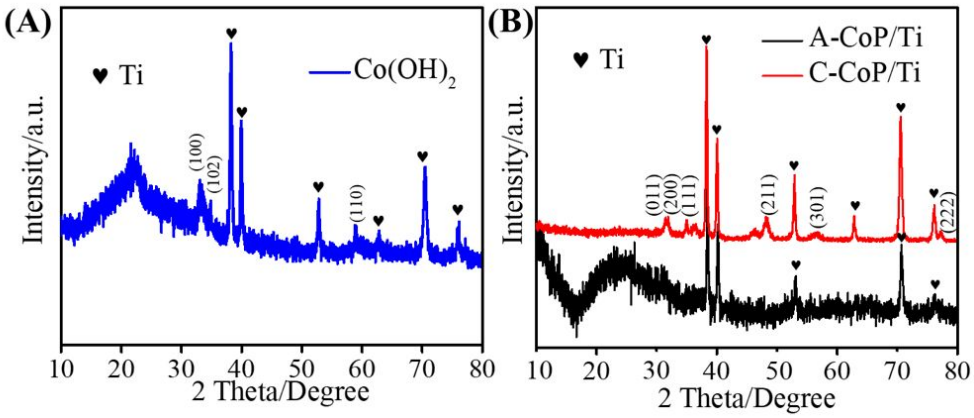

Figure S3. XRD patterns of (A) $Co(OH)_2$/Ti and (B) CoP/Ti.

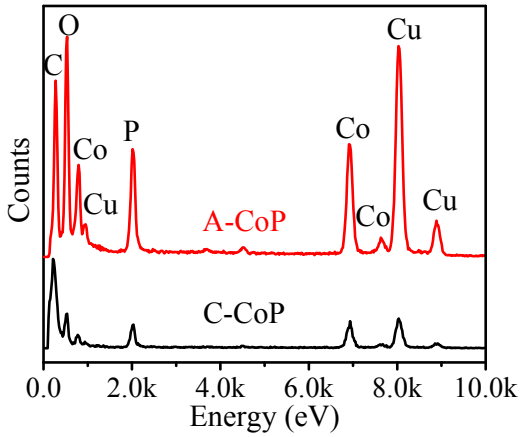

Figure S4. EDX spectra of CoP. Cu and C signal originates from the sample holder.

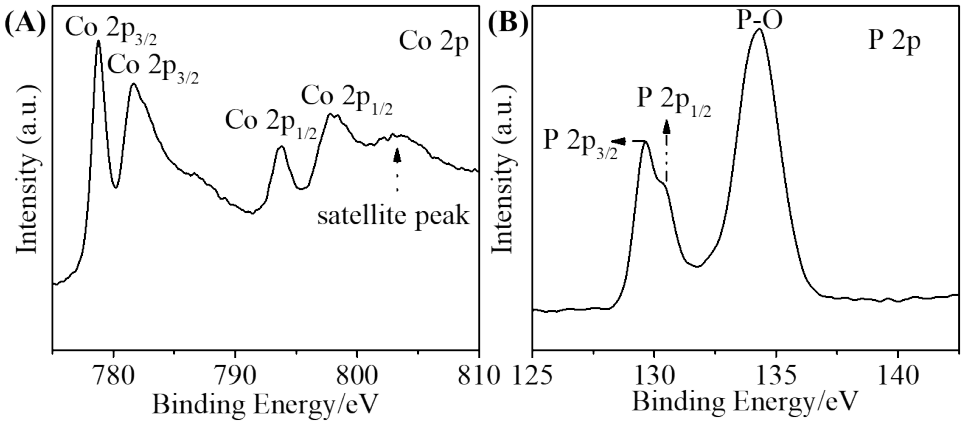

Figure S5. XPS spectra of (A) Co 2p and (B) P 2p in C-CoP.

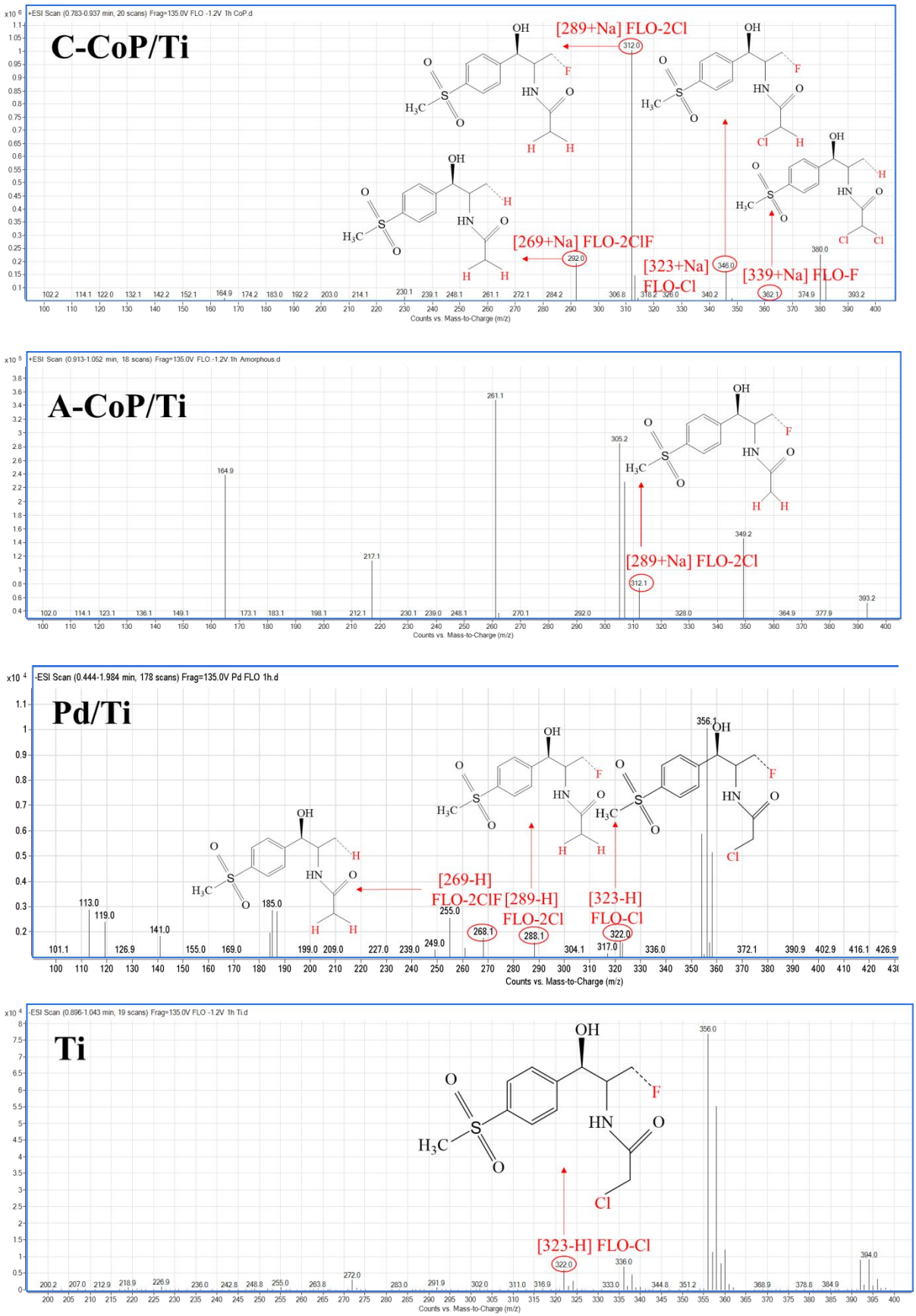

Figure S6. MS identification of FLO dehalogenation products.

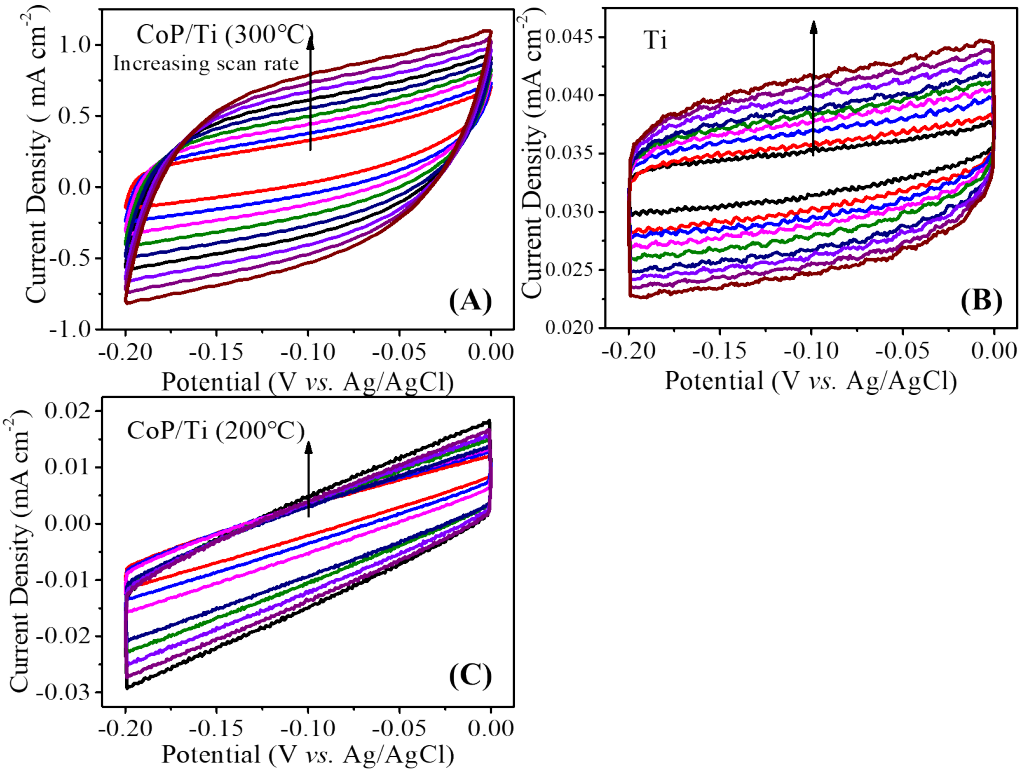

Figure S7. CV curves of (A) C-CoP/Ti, (B) Ti and (C) A-CoP/Ti in the range of 0 ~ -0.20 V vs. Ag/AgCl. The scan rate is 30, 45, 60, 75, 90, 105, 120, 135 and 150 mV s^{-1} for the curves from inside to outside.

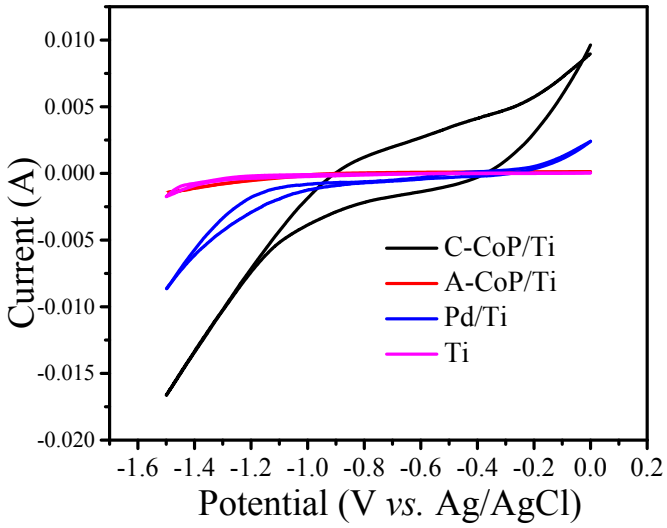

Figure S8. CV spectra of FLO reduction on bare Ti, Pd/Ti, A-CoP/Ti and C-CoP/Ti electrodes (scan rate: 50 mV/s).

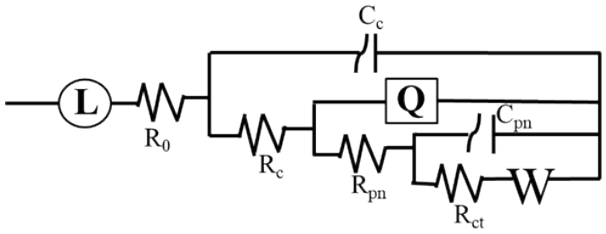

Figure S9. Equivalent circuit used for fitting the Nyquist plots in Figure 2F.

The inductance (*L*) was attributed to high frequency artifacts arising from the apparatus. The resistor (R_0) was the resistance of the electrolyte and the electrodes. Rc and Rpn were the resistance contribution of the solid bulk matrix (Cc) and connected pore network (Q), respectively. Rct denoted to charge transfer resistance/double layer capacitance (Cpn) on the electrode surface and mass/redox transformation within the product/CoP nanosheets layer on the electrode surface. Warburg impedance, *W*, represented diffusion properties. The 45^0 high-frequency intercept is characteristic of the Warburg impedance.

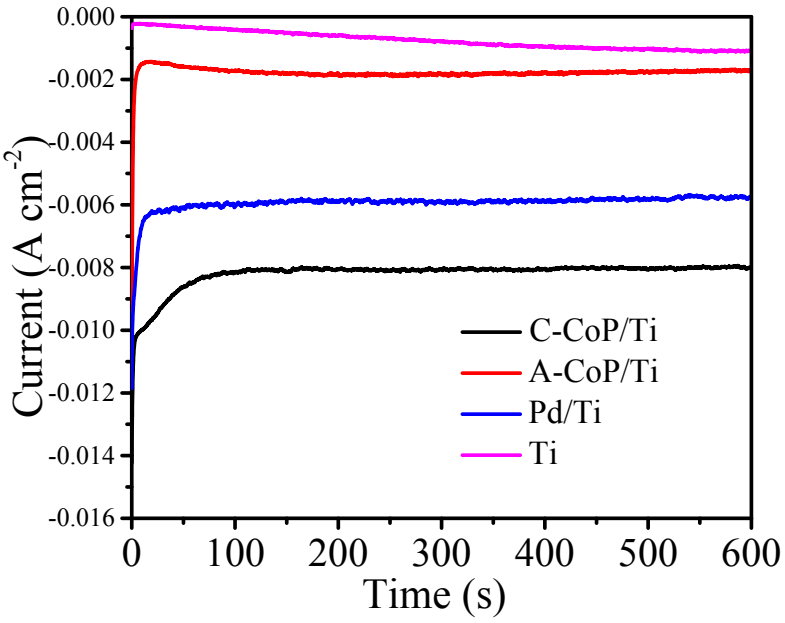

Figure S10. Chronoamperometric profiles at a potential of -1.2 V *vs*. Ag/AgCl on bare Ti, Pd/Ti, A-CoP/Ti and C-CoP/Ti electrodes. Conditions: 0.1 M Na_2SO_4 solution; C_0 = 20 mg L^{-1}; without pH adjustment.

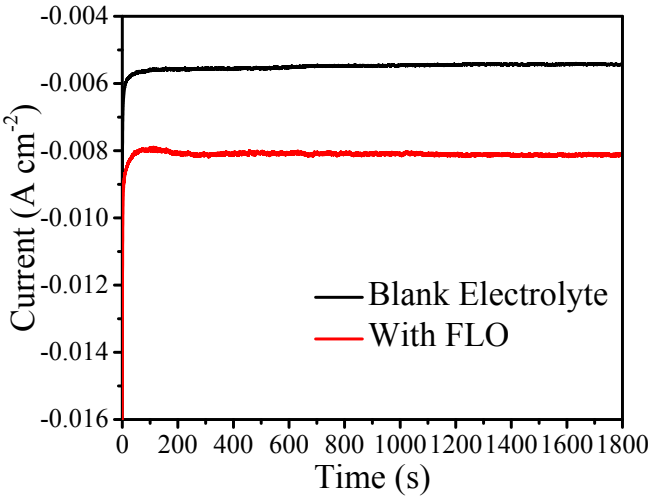

Figure S11. Chronoamperometric profiles at a potential of -1.2 V *vs*. Ag/AgCl for C-CoP/Ti electrode in a blank 0.1 M Na_2SO_4 solution and in 0.1 M Na_2SO_4 solution saturated with FLO (without pH adjustment).

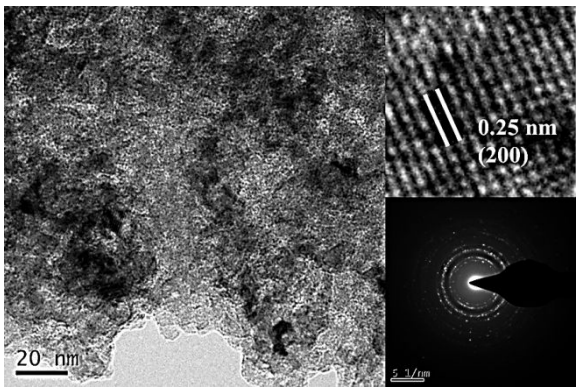

Figure S12. TEM images of the C-CoP nanosheets after 5 circles.

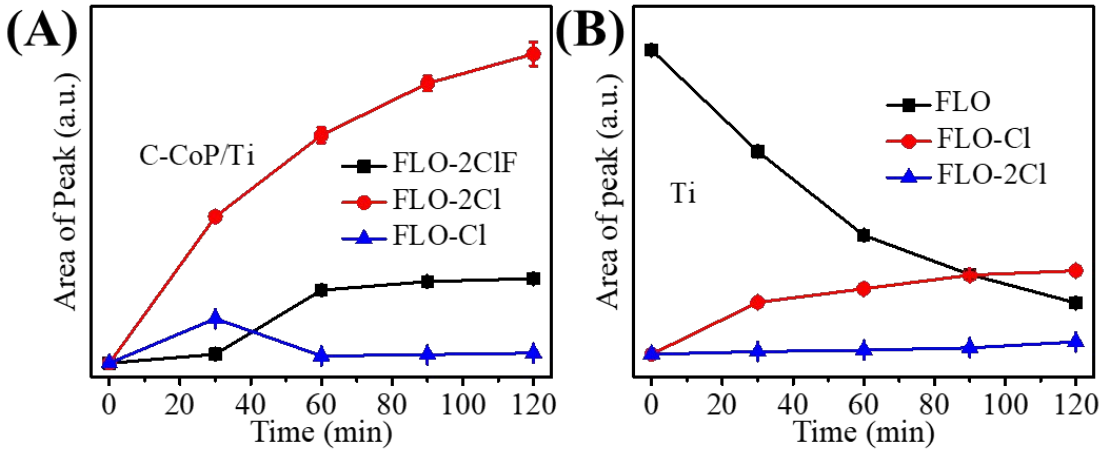

Figure S13. Semi-quantitative analysis of FLO-Cl and FLO-2Cl produced from FLO on C-CoP/Ti and bare Ti electrodes (0.1 M Na_2SO_4 solution; C_0 = 20 mg L^{-1}; –1.2 V *vs*. Ag/AgCl; without pH adjustment.)

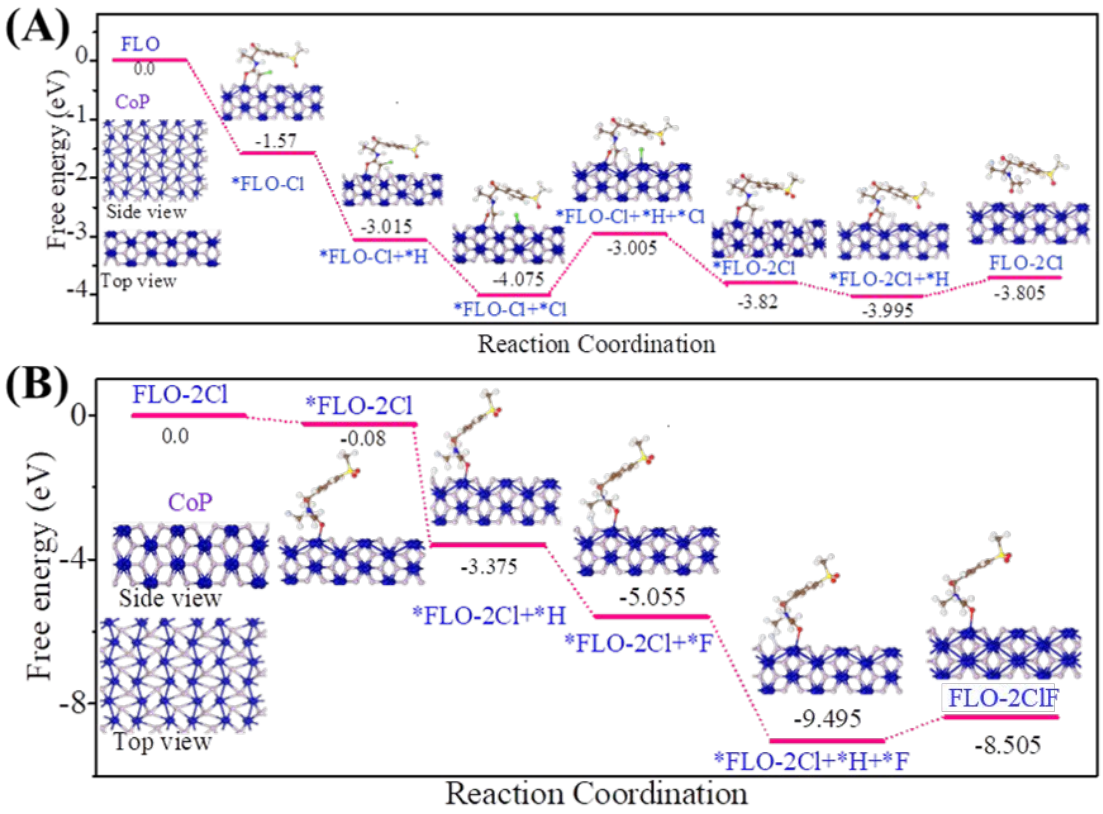

Figure S14. Free energy diagram of the adsorbed FLO molecules in secondary dechlorination (A) and defluorination (B) process on the surface of CoP (200).

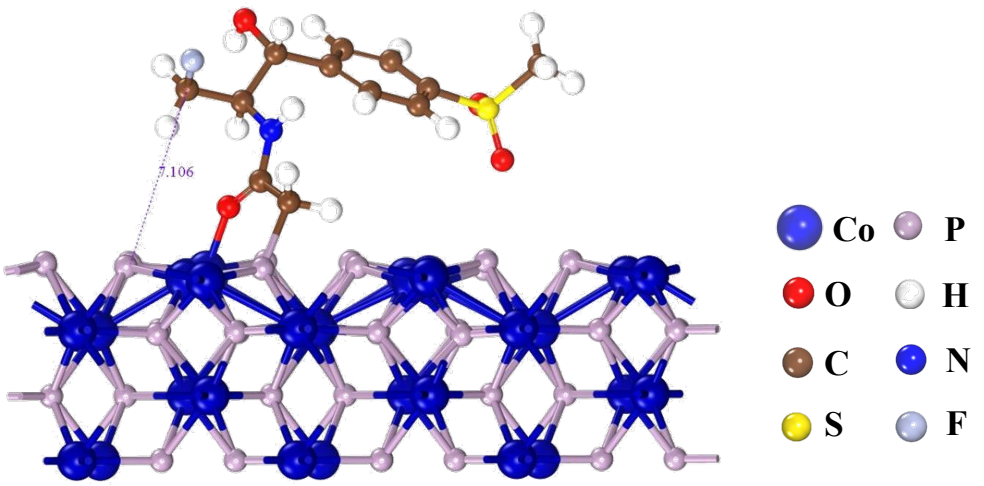

Figure S15. The optimized geometric structure of FLO-2Cl on CoP in a horizontal manner.

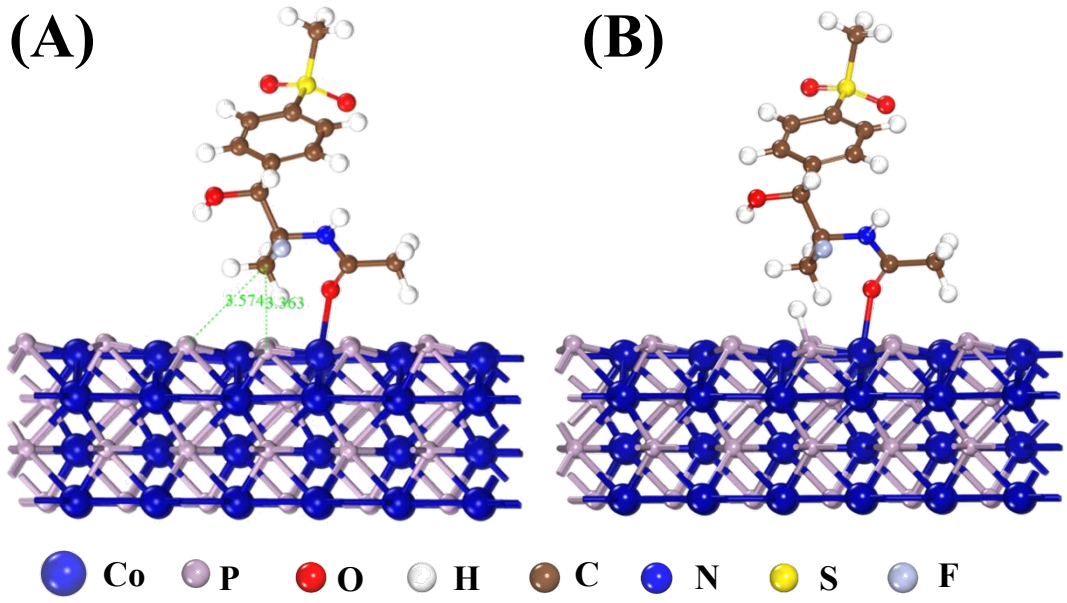

Figure S16. The optimized geometric structures of FLO-2Cl on CoP in a vertical manner: (A) in the absence of H* and (B) in the presence of H*.

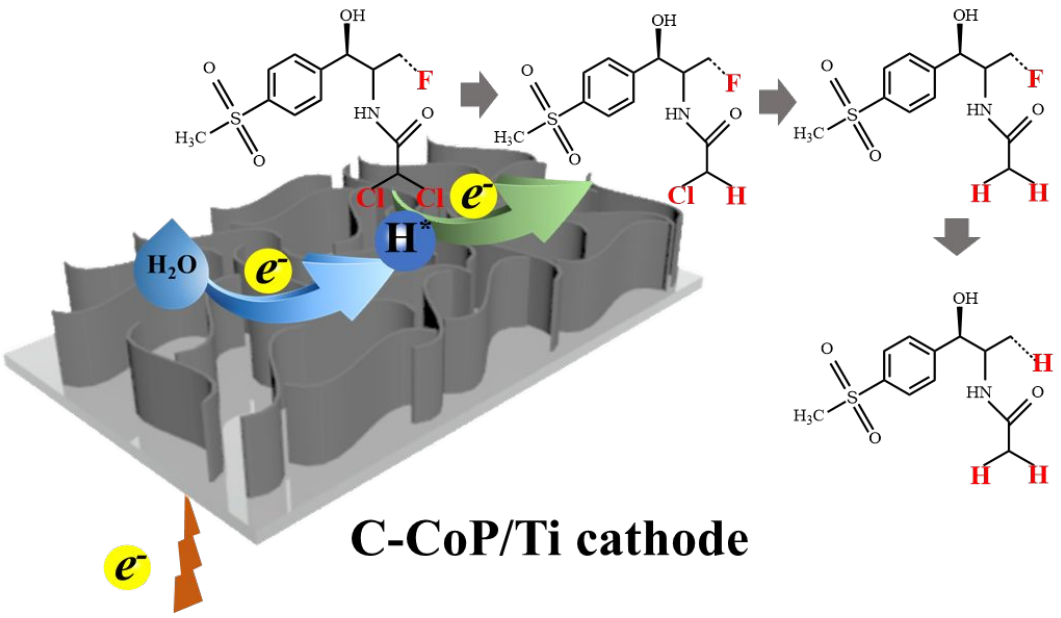

Scheme S1. Schematic dehalogenation pathway of FLO on C-CoP/Ti (plausible mechanism for C-CoP nanosheets electrocatalytic dehalogenation)

Table S1 Electrochemical impedance parameters obtained by fitting the Nyquist plots to the equivalent circuit model (Figure 2F and S9).

Materials	L	R_0	C_c	R_c	Q		R_{pn}	C_{pn}	R_{ct}	W
	H	(Ω)	(nF)	(Ω)	$Y_0(\Omega^{-1}s^n)$	n	(Ω)	(μF)	(Ω)	Y0
C-CoP/Ti	2.575×10^{-19}	3.853	162.3	25.14	1.418×10^{-2}	0.7285	2.582	2.447	1.768×10^{2}	2.043×10^{4}
A-CoP/Ti	1.286×10^{-16}	25.47	1.84×10^{-7}	5.239	1.929×10^{-4}	0.8576	282.5	1.517×10^{-3}	43.4	4.035×10^{-3}
Ti	1.311×10^{-6}	4.163	132.2	1.544	5.145×10^{-4}	0.8463	118.4	4.025×10^{-2}	3.443×10^{4}	6.445×10^{4}

Table S2 Comparison of defluorination activity of different cathode materials.

Cathode materials	Concentration of FLO	Potential (vs. Ag/AgCl)	Proposed mechanism	Time	Defluorination proportion	Ref
C-CoP/Ti	20 mg L^{-1}	-1.2 V	e^-+H*	2 h	21%	This work
Graphite fiber brush	200 mg L^{-1}	-1.25 V	e^-	50 h	29%	1
Co-P/O	20 mg L^{-1}	-1.2 V	e^-+H*+Co-Cl	2 h	-	2
Pd@Ni-foam	20 mg L^{-1}	-1.2 V	e^-+H*	2 h	-	3

Table S3 Quality parameters of real water samples

Water	Taozi Lake	Xiangjiang River
pH	8.05	8.04
TOC (mg L^{-1})	8.348	5.298
Conductivity (mS cm^{-1})	0.347	0.345
Dissolved oxygen (mg L^{-1})	10.02	9.71
Ca^{2+} (mg L^{-1})	26.9	36.6
Na^{+} (mg L^{-1})	12.9	18.0
K^{+} (mg L^{-1})	5.7	3.7
Mg^{2+} (mg L^{-1})	4.9	5.7
Cl^{-} (mg L^{-1})	10.851	13.449
F^{-} (mg L^{-1})	0.478	0.593
NO_3^{-} (mg L^{-1})	3.444	9.902
SO_4^{2-} (mg L^{-1})	34.990	48.969
Removal efficiency (90 min)	97%	98%

REFERENCES

1. Kong, D.; Liang, B.; Yun, H.; Cheng, H.; Ma, J.; Cui, M.; Wang, A.; Ren, N., Cathodic degradation of antibiotics: characterization and pathway analysis. *Water Res* **2015,** *72*, 281-292.

2. . Liu, T.; Luo, J.; Meng, X.; Yang, L.; Liang, B.; Liu, M.; Liu, C.; Wang, A.; Liu, X.; Pei, Y., Electrocatalytic dechlorination of halogenated antibiotics via synergistic effect of chlorine-cobalt bond and atomic H. *J Hazard Mater* **2018,** *358*, 294-301.

3. Yang, L.; Chen, Z.; Cui, D.; Luo, X.; Liang, B.; Yang, L.; Liu, T.; Wang, A.; Luo, S., Ultrafine palladium nanoparticles supported on 3D self-supported Ni foam for cathodic dechlorination of florfenicol. *Chem Eng J* **2019,** *359*, 894-901.